



**HAL**  
open science

## Extending the competitive threshold collision-induced dissociation of Zn(II) ternary complexes using traveling-wave ion mobility-mass spectrometry

Kwabena Senyah, Perfect Asare, Jonathan Wilcox, Federica Angiolari, Riccardo Spezia, Laurence Angel

### ► To cite this version:

Kwabena Senyah, Perfect Asare, Jonathan Wilcox, Federica Angiolari, Riccardo Spezia, et al.. Extending the competitive threshold collision-induced dissociation of Zn(II) ternary complexes using traveling-wave ion mobility-mass spectrometry. *International Journal of Mass Spectrometry*, 2023, 488, pp.117041. 10.1016/j.ijms.2023.117041 . hal-04082966

**HAL Id: hal-04082966**

**<https://hal.science/hal-04082966>**

Submitted on 26 Apr 2023

**HAL** is a multi-disciplinary open access archive for the deposit and dissemination of scientific research documents, whether they are published or not. The documents may come from teaching and research institutions in France or abroad, or from public or private research centers.

L'archive ouverte pluridisciplinaire **HAL**, est destinée au dépôt et à la diffusion de documents scientifiques de niveau recherche, publiés ou non, émanant des établissements d'enseignement et de recherche français ou étrangers, des laboratoires publics ou privés.

**Extending the competitive threshold collision-induced dissociation of Zn(II) ternary complexes  
using traveling-wave ion mobility-mass spectrometry**

Kwabena Senyah,<sup>a</sup> Perfect Asare,<sup>a</sup> Jonathan Wilcox,<sup>a</sup> Federica Angiolari,<sup>b</sup> Riccardo Spezia,<sup>b</sup> Laurence A.  
Angel<sup>a\*</sup>

<sup>a</sup> *Department of Chemistry, Texas A&M University-Commerce, 2600 S Neal Street, Commerce, TX,  
75428, USA*

<sup>b</sup> *Laboratoire de Chimie Théorique, Sorbonne Université, UMR 7616 CNRS, 4, Place Jussieu, 75005  
Paris, France*

**Keywords:** threshold collision-induced dissociation; Synapt TCID; zinc ternary complexes; immobilized metal affinity chromatography; peptide tags; alternative metal binding peptide.

\*Corresponding author: Dr. Laurence Angel, Department of Chemistry, Texas A&M University-Commerce, 2600 S Neal St., Commerce, TX, 75428, USA, E-mail: Laurence.Angel@tamuc.edu

## Abstract

The competitive threshold collision-induced dissociation (TCID) of the ternary complex  $[\text{amb}_5+\text{Zn(II)}+\text{NTA}]^- \rightarrow [\text{amb}_5+\text{Zn(II)}]^- + \text{NTA}$  or  $\rightarrow [\text{NTA}+\text{Zn(II)}]^- + \text{amb}_5$ , where  $\text{amb}_5 = \text{His-Cys-Gly-Pro-Gly-Gly-Cys}$  or  $\text{Asp-His-Gly-Pro-Gly-Gly-Cys}$  and NTA = nitrilotriacetic acid, were studied using traveling-wave ion mobility-mass spectrometry (TWIMMS). The analyses included calculating the reaction cross sections as a function of center-of-mass collision energy at three pressures of the argon collision gas, which covers the pressure range available in the TWIMMS instrument. The ternary complex contained one of the  $\text{amb}_5$  peptides, whose His, Cys and/or Asp substituent groups could compete with the NTA carboxylate sites for binding Zn(II). A new molecular modeling procedure was developed, initially using PM6 geometry-optimizations and thermochemical analyses to locate low-energy conformers of the ternary complex and its products that also had collision cross sections ( $\Omega_{\text{He}}$ ), measured using the ion size scaled Lennard-Jones (L-J) method, that were close to the TWIMMS measured  $\Omega_{\text{He}}$ . A selection of these conformers were further geometry-optimized at the DFTB/3OB\_D4 level of theory and using these as starting structures, molecular dynamics (MD) simulations were conducted to sample the ensemble of structures L-J  $\Omega_{\text{He}}$  at 300 K. From these analyses, a selection of reactant and product conformers whose L-J  $\Omega_{\text{He}}$  best matched the TWIMMS  $\Omega_{\text{He}}$  were used in the TCID fitting of the center-of-mass energy-dependent, reaction cross sections extrapolated to zero pressure. The TCID fitting determined the threshold energies of the two product channels which in the absence of an activation barrier in excess of the energy of the products equates to the 0 K dissociation enthalpies ( $\Delta H_0$ ). The difference in  $\Delta H_0$  for the two competing reactions allowed for a relative gas-phase Zn(II) affinity scale to be constructed for the  $\text{amb}_5$  peptides studied here and from our previous published  $\text{amb}_5$  research.

## Introduction

The competitive threshold collision-induced dissociation (TCID) method, developed by Armentrout, Ervin and Rodgers,<sup>1-3</sup> is a reaction dynamics method for obtaining the thermochemistry of competing reactions driven by the collision between the reactant and an inert collision gas, and is applied through the CRUNCH program.<sup>4</sup> The competitive TCID method has been applied to a variety of chemical systems including ionic liquid clusters,<sup>5,6</sup> protonated tripeptides,<sup>7,8</sup> sodium cation complexes,<sup>9</sup> and the gas-phase proton affinities organic molecules.<sup>10-14</sup> Recently we have shown a competitive TCID approach for studying a series of alternative metal binding (amb) peptides, which was applied to the competitive dissociation of the [amb+Zn(II)+NTA]<sup>-</sup> ternary complex:<sup>15,16</sup> an original application due to the ternary complexes relatively large size and the use of the traveling-wave ion mobility-mass spectrometry (TWIMMS) platform.<sup>17</sup> The research presented here further extends the TCID instrumental and theoretical approaches applied to the TWIMMS platform and provides the thermochemistry and relative Zn(II) affinity for two new amb<sub>5</sub> species (Fig 1) and compares them with our previous results. This new TCID research, includes converting ion intensities into product reaction cross sections ( $\sigma_p$ ) which are extrapolated to the single collision limit, and the application of a new theoretical approach for selecting the reactant and product conformers to use in the TCID modeling. Notably, we have used theoretical calculations to identify the structures of the ions by comparing theoretical with experimental collision cross sections. This was done in two ways: (i) using the structures resulting from geometry optimization; (ii) using an ensemble of structures sampled by molecular dynamics simulations. The first approach is what is typically done, while the second one was much less used. Typically classical molecular dynamics (MD) simulations were done in the past improve the collision cross sections of large macromolecules,<sup>18,19</sup> while here we used first-principles MD simulations using tight-binding Density Functional Theory in order to correctly consider the Zn(II) binding and allowing possible proton transfers.

Our previous research of the amb peptides showed that by preparing their samples in a series of acidic to basic pH solutions that pH-dependent metal binding was observed and by changing residues in

their primary structure the specificity for chelating different metal ions could be adapted.<sup>20-29</sup> Some of the most extensive metal binding research was on a series of amb<sub>5</sub> heptapeptides,<sup>15,16,22,24,26,28</sup> named in alphabetical order amb<sub>5A</sub> to amb<sub>5R</sub>, which were designed to explore the primary structure acetyl-Aa<sub>1</sub>-Aa<sub>2</sub>-Gly<sub>3</sub>-Pro<sub>4</sub>-Tyr<sub>5</sub>-Aa<sub>6</sub>-Aa<sub>7</sub>, where the Aa were different combinations of His, Cys or Asp that have metal binding substituent groups. The central residues provided a spacer, a hinge, and  $\pi$ -metal ion interaction. However, the previous Zn(II) binding studies indicated that it was the substituent group in the Aa<sub>1</sub>-Aa<sub>2</sub>-Aa<sub>7</sub> positions with the carboxylate at the terminus that provided the distorted tetrahedral Zn(II) coordination.<sup>24,27</sup> Here we extend this series with simplified primary structures for amb<sub>5S</sub> and amb<sub>5T</sub> (Fig 1) which have alternative Aa<sub>1</sub>-Aa<sub>2</sub>-Aa<sub>7</sub> binding sites for forming the binary [amb<sub>5</sub>+Zn(II)]<sup>-</sup> and ternary [amb<sub>5</sub>+Zn(II)+NTA]<sup>-</sup> complexes but replace the sites at Tyr<sub>5</sub>-Aa<sub>6</sub> with Gly<sub>5</sub>-Gly<sub>6</sub>, which will test whether the Tyr<sub>5</sub>  $\pi$ -zinc ion interaction or the Aa<sub>6</sub> substituent sites were significant in our previous Zn(II) binding studies. The overall 1- charge state of the complexes are determined by the oxidation state of Zn(II) and the protonation states of the weak acid or basic sites of the amb<sub>5</sub> and/or NTA, relating to 3 negatively-charged sites, *i.e.*, [amb<sub>5</sub>-H+Zn(II)+NTA-2H]<sup>-</sup>, [amb-3H+Zn(II)]<sup>-</sup> or [NTA-3H+Zn(II)]<sup>-</sup>. In the following script, the '-3H' is omitted from the names of the complexes, but the descriptions of the molecular modeling results include a discussion of the protonation states in these complexes.

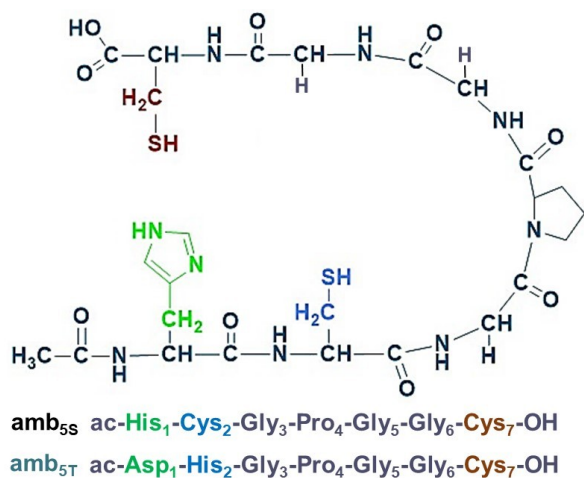


**Figure 1.** The primary structures of the alternative metal binding amb<sub>5S</sub> and amb<sub>5T</sub> peptides with the potential metal-binding of the substituent groups of His, Cys or Asp in the first, second and last positions shown in green, blue and brown.

## 1. Experimental, computational and molecular modeling methods

### 2.1 Reagents and preparation of the ternary complexes

The peptides ac-His-Cys-Gly-Pro-Gly-Gly-Cys (amb<sub>SS</sub>) and ac-Asp-His-Gly-Pro-Gly-Gly-Cys (amb<sub>ST</sub>) were synthesized by PepmicCo (<http://www.pepmic.com/>). Zinc(II) nitrate hexahydrate (99%+ purity) was acquired from Alfa Aesar ([www.alfa.com/](http://www.alfa.com/)). Ammonium hydroxide (trace metal grade) and ammonium acetate (ultrapure) were acquired from Fisher Scientific (<http://www.Fishersci.com/>) and VWR (<https://us.vwr.com/>), respectively. Stock and working solutions were made with deionized water >17.8 MΩ cm (<http://www.millipore.com>) and HPLC grade methanol (<http://www.Fishersci.com/>). The [amb<sub>5</sub>+Zn(II)+NTA]<sup>-</sup> complex was prepared by combining the zinc nitrate hexahydrate with the NTA followed by the addition of the amb<sub>5</sub> and then 50% methanol in DI water. Further dilution with DI water produced samples with final concentrations of 25.0 μM amb<sub>5</sub> or Zn(II) and 50.0 μM NTA in 10% methanol aqueous solution. The solutions were thoroughly mixed and left at room temperature for 10 minutes. The final solutions had a pH 2.8-3.0.

### 2.2 Threshold collision-induced dissociation of the ternary complex

The instrumental analyses were conducted using the Waters Synapt G1 instrument<sup>17</sup> (Fig S1) using operating conditions as described in the Supporting Information. The negatively-charged [amb<sub>5</sub>+Zn(II)+NTA]<sup>-</sup> complex was resolved by the transmission quadrupole, collected in the trap and injected with a 200 μs gate into the ion mobility traveling-wave (IM T-wave) cell. The [amb<sub>5</sub>+Zn(II)+NTA]<sup>-</sup> ions underwent about 10,000 collisions with the nitrogen buffer gas before acceleration into the transfer T-wave cell using predetermined collision energies (CE). The dissociation of the complex in the transfer T-wave meant the product ions had the same arrival time distribution (ATD) as the precursor [amb<sub>5</sub>+Zn(II)+NTA]<sup>-</sup> complex, and only those were included in the analyses.<sup>15,16</sup> The ternary complex and product ions were identified using the TOF mass analyzer operated in V-mode by their *m/z* isotope patterns. Analyses of the data was conducted using the Driftscope 2.0 and MassLynx 4.1 softwares. The

ATDs were extracted from the Driftscope 2.0 software and the area under each of the ATDs were integrated to determine the relative intensities of the precursor and products ions. The procedure was repeated for a series of transfer CE that included the range that covered the 0-100% dissociation of the  $[\text{amb}_5+\text{Zn(II)}+\text{NTA}]^-$ . Moreover, each series of CE were repeated using three argon collision gas pressures, covering the upper and lower pressure range available from the Synapt G1 instrument.

### 2.3 Collision cross sections

In separate experiments, with the quadrupole in non-resolving mode and no transfer CE, the collision cross sections (CCS) of the  $[\text{amb}_5+\text{Zn(II)}+\text{NTA}]^-$  and  $[\text{amb}_5+\text{Zn(II)}]^-$  complexes were measured using D-L polyalanine calibrants to make a calibration curve to convert the ATDs of the  $\text{amb}_5$  complexes into CCS as measured in helium buffer gas ( $\Omega_{\text{He}}$ ). The measurement of  $\Omega_{\text{He}}$  allowed the comparison of the TWIMMS measured  $\Omega_{\text{He}}$  with the geometry-optimized conformations found by the molecular modeling, where their  $\Omega_{\text{He}}$  were calculated by the Lennard-Jones (L-J) ion size scaled method using the Sigma program.<sup>30</sup> Details of these methods are described in the Supporting Information.

### 2.4 Molecular modeling of $[\text{amb}_5+\text{Zn(II)}+\text{NTA}]^-$ conformers and their products

An initial study for locating a series of geometry-optimized conformers of the negatively charged  $[\text{amb}_5+\text{Zn(II)}+\text{NTA}]^-$  complexes and their products was conducted using the semi-empirical PM6 method<sup>31</sup> from Gaussian09,<sup>32</sup> using starting structures with structural modifications to test which combination of the His, Cys or Asp substituent groups and the NTA carboxyl groups would optimize to give the lowest-energy conformers that also had L-J  $\Omega_{\text{He}}$  (measured with an average of 200 measurements using the Sigma program with an accuracy set at 0.5%) that were close to the experimental TWIMMS  $\Omega_{\text{He}}$ . From these initial results, a selection of conformers that exhibited these criteria but had different binding configurations were further geometry-optimized using tight-binding Density Functional Theory (DFTB) using the 3OB Slater-Koster parameters with third order corrections<sup>33-35</sup> and D4 dispersion corrections<sup>36,37</sup> (hereafter called 3OB\_D4), their L-J  $\Omega_{\text{He}}$  were measured before molecular dynamics (MD) simulations

were conducted using these DFTB/3OB\_D4 conformers (5 ps equilibrium and 20-50 ps dynamics with L-J  $\Omega_{\text{He}}$  set to 0.5 % to do a single calculation for each structure extracted from MD simulations) to obtain the distribution and average L-J  $\Omega_{\text{He}}$  of the conformer at 300 K. In this way, the standard deviation obtained from multiple estimations of L-J  $\Omega_{\text{He}}$  of one structure is smaller than the standard deviation on L-J  $\Omega_{\text{He}}$  obtained from a conformational sampling. The temperature was controlled by a Langevin thermostat with a friction coefficient of 0.01 fs<sup>-1</sup> (in the equilibration portion a higher friction coefficient, 0.1 fs<sup>-1</sup>, was used) and an integration time step of 1 fs was used. Simulations were done using our in-house code<sup>38</sup> which uses the integration scheme proposed by Ceriotti et al.<sup>39</sup> enabling us to include nuclear quantum effects via the Ring Polymer Molecular Dynamics method<sup>40</sup> with a mild thermostat on the beads, while a classical trajectory is recovered when the number of beads (P) is set to 1. Here we used P=1 for all the trajectories except for one case in which P=8 was also used. The dynamics routine is coupled with DFTB+ software to obtain energies and gradients.<sup>41</sup>

### 2.5 Center-of-mass collision energy and product reaction cross sections

The lab-frame collision energy ( $E_{\text{lab}}$ ) applied to the transfer cell was converted to center-of-mass collision energy  $E_{\text{cm}}$  using the average mass of the argon ( $m_{\text{Ar}}$ ) collision gas and the average mass of the [amb<sub>5</sub>+Zn(II)+NTA]<sup>-</sup> ternary complex ( $m_{\text{TC}}$ ) by equation 1.

$$E_{\text{cm}} = E_{\text{lab}} m_{\text{Ar}} / (m_{\text{Ar}} + m_{\text{TC}}) \quad (1)$$

where  $E_{\text{cm}}$  is the average energy converted from the collision into internal energy of the ternary complex and available for the dissociation reaction. The  $E_{\text{cm}}$ -dependent intensities of the product ions are converted to reaction cross sections using Beer's law from the total ( $I_0$ ) and transmitted ( $I$ ) reactant ion intensities<sup>42</sup>

$$I = I_0 \exp(-\sigma_{\text{tot}}nl) \quad (2)$$

where  $\sigma_{\text{tot}}$  is the total reaction cross section,  $n$  is the argon gas density,  $l$  is the path length of the transfer collision cell (10.0 cm) and  $I_0$  is determined from

$$I_0 = I + \sum I_p \quad (3)$$

and includes the sum of the two product ion intensities  $I_p$  produced by the reactions. The individual product reaction cross sections ( $\sigma_p$ ) are given by

$$\sigma_p = \sigma_{\text{tot}} (I_p / \sum I_p) \quad (4)$$

## 2.6 CRUNCH analyses using the competitive threshold collision induced dissociation method

The competitive TCID model for simultaneously fitting the two competing  $E_{\text{cm}}$ -dependent product reaction cross sections<sup>1,2</sup> was applied via the CRUNCH program.<sup>4</sup> The TCID model includes (1) internal energy distribution of the  $[\text{amb}_5 + \text{Zn(II)} + \text{NTA}]^-$  complex,<sup>43</sup> (2) convolution over translational energy distributions of the collision between  $[\text{amb}_5 + \text{Zn(II)} + \text{NTA}]^-$  and the Ar collision gas,<sup>44</sup> (3) statistical RRKM rate constants into the two product channels and correction of the kinetic shifts due to the 50  $\mu\text{s}$  time window from the collision cell to the TOF detector,<sup>3</sup> and (4) integration over the total rotational angular momentum  $J$  levels.<sup>14,45</sup>

The probability of dissociation and detection of the energized ternary complex with total energy  $E^*$  to product channel  $j$  is given by first-order reaction kinetics of two product channels using equation 5.

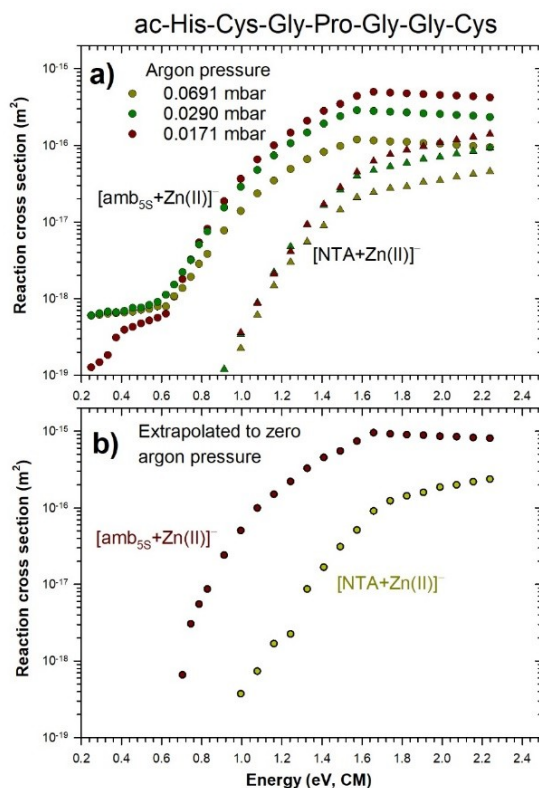
$$P_{D,j}(E^*, J) = k_j(E^*, J) / k_{\text{tot}}(E^*, J) [1 - \exp(-k_{\text{tot}}(E^*, J)\tau)] \quad (5)$$

where  $k_{\text{tot}} = \sum k_j$  is the total dissociation rate constant of the individual channels  $j$  and  $\tau$  is the time-of-flight of the center-of-mass of the system from the collision cell to the mass spectrometer detector.<sup>2,3</sup>  $J$  is the angular momentum quantum number for the rotational energies of the energized molecule and orbiting transition-state configuration. The long-range potential, using molecular polarizabilities and dipole moments of the neutral species, describes the ion-induced-dipole interaction as a locked dipole.<sup>45</sup> These analyses require vibrational and rotational frequencies for the reactant and products and the polarizabilities and dipole moments for the neutral products taken from the PM6 or DFTB calculations or the NIST database. The complete evaluation of the energies available for the dissociation of the ternary complex into the two product channels allows for the thermochemical analyses of these reactions.

## Results and Discussion

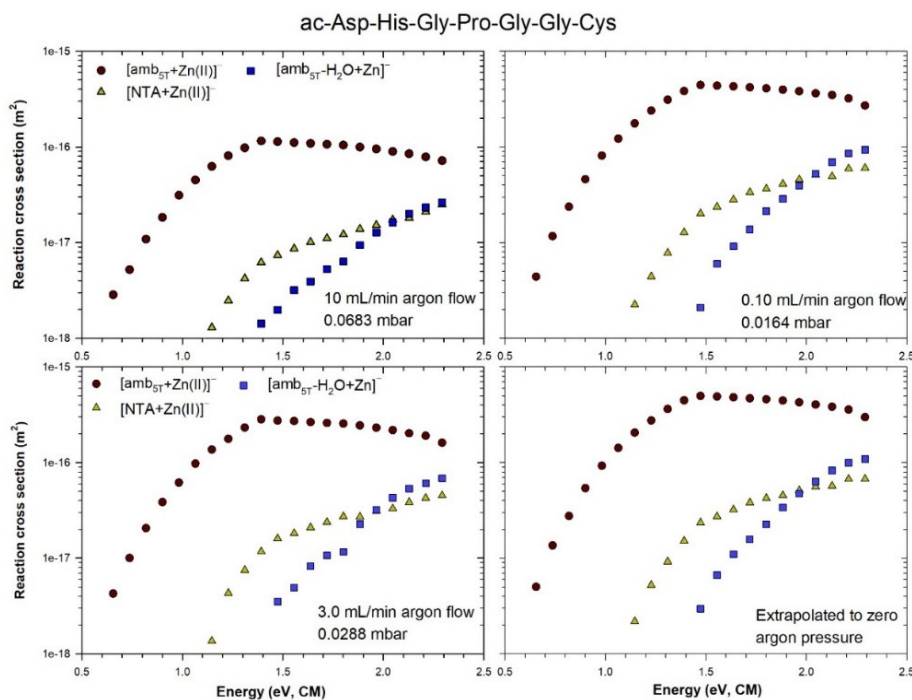
### 3.1 The collision gas pressure dependence on the products reaction cross sections

Figure 2a shows the two product reaction cross sections ( $\sigma_p$ ) for  $[\text{amb}_{55}+\text{Zn(II)}]^-$  and  $[\text{NTA}+\text{Zn(II)}]^-$  that were produced by the TCID of  $[\text{amb}_{55}+\text{Zn(II)}+\text{NTA}]^-$  taken at three argon gas pressures and the polynomial extrapolation of the  $\sigma_p$  using the three gas pressures to the single collision limit (Fig 2b). The  $\sigma_p$  of  $[\text{amb}_{55}+\text{Zn(II)}]^-$  (Fig 2a) over the lowest  $E_{\text{cm}} = 0.2\text{-}0.6$  eV, exhibited elevated  $\sigma_p$  that were directly dependent on the pressure of the argon gas, a feature not observed in our previous TCID studies.<sup>15,16</sup> A polynomial extrapolation of the  $\sigma_p$  to the zero argon pressure limit, removed this feature (Fig 2b) and produced well-defined threshold regions for the  $[\text{amb}_{55}+\text{Zn(II)}]^-$  and  $[\text{NTA}+\text{Zn(II)}]^-$  product channels.



**Figure 2.** The threshold collision-induced dissociation of  $[\text{amb}_{55}+\text{Zn(II)}+\text{NTA}]^-$  showing **a)** the reaction cross sections for the product channels  $[\text{amb}_{55}+\text{Zn(II)}]^-$  and  $[\text{NTA}+\text{Zn(II)}]^-$  taken at argon gas pressures of 0.0691 mbar, 0.0290 mbar, and 0.0171 mbar, and **b)** the polynomial extrapolation of the reaction cross sections to zero argon gas pressure at the single collision limit.

Over the higher  $E_{cm} = 0.6\text{-}2.4$  eV CE range, the  $\sigma_p$  exhibited an *increase* as argon gas pressures *decreased*, resulting in the overall increase in  $\sigma_p$  from the polynomial extrapolation (Fig 2b). This increase in reactivity may be explained because the initial collision of the accelerated ternary complex with an argon atom is most precisely controlled by the applied transfer collision energy when the ternary complex has an initial collision-free path that allows it to accelerate to the applied transfer collision energy before the initial collision. However, if there are multiple collisions along this initial path then these generally are less energetic because the complex does not have enough time between collisions to accelerate to the full applied collision energy. Subsequently these lower energy multiple collisions can result with less internal excitation of the ternary complex. Moreover, lower energy multiple collisions inside the transfer T-wave cell can result with some of the initial internal excitation energy from the initial collision being removed, resulting in partial deactivation of the ternary complex, both these mechanisms will be most pronounced at the higher argon gas pressures.



**Figure 3.** The threshold collision-induced dissociation of  $[\text{amb}_{5T}+\text{Zn}(\text{II})+\text{NTA}]^-$  showing the reaction cross sections for the product channels of  $[\text{amb}_{5T}+\text{Zn}(\text{II})]^-$ ,  $[\text{NTA}+\text{Zn}(\text{II})]^-$  and  $[\text{amb}_{5T}-\text{H}_2\text{O}+\text{Zn}(\text{II})]^-$  at collision gas pressures of **a)** 0.0683 mbar argon, **b)** 0.0288 mbar argon, **c)** 0.0164 mbar argon in the transfer collision cell, and **d)** the linear extrapolation of the reaction cross section to zero argon gas pressure at the single collision limit.

Figure 3 shows the  $\sigma_p$  versus  $E_{cm}$  from the TCID of  $[\text{amb}_{5T}+\text{Zn(II)}+\text{NTA}]^-$  producing the  $[\text{amb}_{5T}+\text{Zn(II)}]^-$ ,  $[\text{NTA}+\text{Zn(II)}]^-$  and  $[\text{amb}_{5T}-\text{H}_2\text{O}+\text{Zn(II)}]^-$  channels, the last channel being the sequential dissociation of  $[\text{amb}_{5T}+\text{Zn(II)}]^-$  through the loss of a water molecule from  $\text{amb}_{5T}$ . The results from the three different argon gas pressures in the transfer collision cell (Fig 3a, b, and c) show the  $\sigma_p$  exhibit a systematic *increase* as the argon gas pressure *decreased* over 0.0683 mbar, 0.0288 mbar to 0.0164 mbar, indicating fewer collisions increased the reactivity of the activated complex (see discussion above). Therefore, the linear extrapolation of the  $\sigma_p$  using the three pressures to the single-collision limit (Fig 3d) increased the  $\sigma_p$  over the whole  $E_{cm} = 0.6\text{-}2.4$  eV region and produced well-defined threshold regions for all three product ions.

### 3.2 Conformers of $[\text{amb}_5+\text{Zn(II)}+\text{NTA}]^-$ complexes and the dissociation products

A new theoretical approach was used to locate the conformers of  $[\text{amb}_5+\text{Zn(II)}+\text{NTA}]^-$  and their dissociation products  $[\text{amb}_5+\text{Zn(II)}]^- + \text{NTA}$  and  $[\text{NTA}+\text{Zn(II)}]^- + \text{amb}_5$  to use in the TCID modeling of these reactions. The semi-empirical PM6 method was used to explore a wide range of conformers of the reactants and products, where the peptide bonds for the  $\text{amb}_5$  species were kept in their *trans* configurations<sup>22</sup> with different arrangements of the potential binding sites of His, Cys, Asp and the carboxyl groups. Table 1 shows the L-J  $\Omega_{\text{He}}$  of a selection of different Zn(II) binding motifs located by PM6 that exhibited the lowest-energy thermochemical analyses and L-J  $\Omega_{\text{He}}$  close to the  $\Omega_{\text{He}}$  measured by TWIMMS. These conformers were further geometry-optimized at DFTB/3OB\_D4 level of theory and their L-J  $\Omega_{\text{He}}$  measured to compare to the TWIMMS  $\Omega_{\text{He}}$ . Using the DFTB/3OB\_D4 geometry-optimized conformers as starting geometry, MD simulations were conducted at 300 K and 500 conformers were extracted over the 50 ps time-frame of the simulations to measure their distributions and average L-J  $\Omega_{\text{He}}$  and locate which of the conformers compared best with the TWIMMS  $\Omega_{\text{He}}$  and select those to use in the TCID modeling.

**Table 1.** Comparison of the average TWIMMS  $\Omega_{\text{He}}$  ( $\text{\AA}^2$ ) and the L-J  $\Omega_{\text{He}}$  of selected low-energy stationary states (static) initially located by geometry-optimizations and thermochemical analyses by PM6, further geometry-optimized by DFTB/3OB\_D4 (DFTB static), and molecular dynamics simulations of the DFTB conformers at 300 K (DFTB-MD). The PM6 conformers are shown in Figures S2 to S7 in the Supporting Information and are identified in the Table. The bold values show the  $[\text{amb}_5+\text{Zn(II)+NTA}]^-$  and  $[\text{amb}_5+\text{Zn(II)}]^-$  conformers with L-J  $\Omega_{\text{He}}$  that best agreed with the TWIMMS  $\Omega_{\text{He}}$  and the  $\text{amb}_5$  with the lowest thermochemical analyses, selected to use in the TCID modeling.

	$[\text{amb}_{5\text{S}}+\text{Zn(II)+NTA}]^-$			$[\text{amb}_{5\text{S}}+\text{Zn(II)}]^-$			$\text{amb}_{5\text{S}}$	
TWIMMS	196 $\pm$ 4			168 $\pm$ 3			-	
	S2a	S2b	<b>S2c</b>	S3a	S3b	<b>S3c</b>	<b>S4a</b>	S4b
PM6 static	194 $\pm$ 1	204 $\pm$ 1	<b>195 <math>\pm</math> 1</b>	174 $\pm$ 1	163 $\pm$ 1	<b>168 <math>\pm</math> 1</b>	<b>169 <math>\pm</math> 1</b>	166 $\pm$ 1
DFTB static	187 $\pm$ 1	199 $\pm$ 1	<b>197 <math>\pm</math> 1</b>	175 $\pm$ 1	163 $\pm$ 1	<b>163 <math>\pm</math> 1</b>	<b>165 <math>\pm</math> 1</b>	165 $\pm$ 1
DFTB-MD	192 $\pm$ 2	203 $\pm$ 3	<b>196 <math>\pm</math> 2</b>	174 $\pm$ 3	163 $\pm$ 3	<b>166 <math>\pm</math> 2</b>	<b>169 <math>\pm</math> 3</b>	169 $\pm$ 2
	$[\text{amb}_{5\text{T}}+\text{Zn(II)+NTA}]^-$			$[\text{amb}_{5\text{T}}+\text{Zn(II)}]^-$			$\text{amb}_{5\text{T}}$	
TWIMMS	195 $\pm$ 4			166 $\pm$ 3			-	
	S5a	<b>S5b</b>	S5c	S6a	<b>S6b</b>	-	S7a	<b>S7b</b>
PM6 static	207 $\pm$ 1	<b>196 <math>\pm</math> 1</b>	207 $\pm$ 1	170 $\pm$ 1	<b>167 <math>\pm</math> 1</b>	-	173 $\pm$ 1	<b>175 <math>\pm</math> 1</b>
DFTB static	199 $\pm$ 1	<b>196 <math>\pm</math> 1</b>	204 $\pm$ 1	169 $\pm$ 1	<b>168 <math>\pm</math> 1</b>	-	173 $\pm$ 1	<b>173 <math>\pm</math> 1</b>
DFTB-MD	202 $\pm$ 2	<b>201 <math>\pm</math> 3</b>	209 $\pm$ 2	175 $\pm$ 4	<b>167 <math>\pm</math> 3</b>	-	170 $\pm$ 3	<b>174 <math>\pm</math> 3</b>

Notably, the average  $\Omega_{\text{He}}$  values obtained from MD simulations, shown in Table 1, are in agreement with experiments, and they are similar or slightly different (mostly larger) than what was obtained from the corresponding optimized geometries. For the  $\text{amb}_{5\text{T}}$  peptide using the S7a initial geometry, we have run simulations including nuclear quantum effects and the calculated  $\Omega_{\text{He}} = 174 \pm 4 \text{\AA}^2$  was slightly larger than the classical one, but inside the statistical uncertainty. Since these calculations are much more computationally expensive and the difference is not so important for all the other systems we consider here only the Newtonian trajectories.

The sampling of the ensemble structures from the MD simulations allowed the L-J  $\Omega_{\text{He}}$  distributions of the conformers of  $[\text{amb}_5+\text{Zn(II)+NTA}]^-$  and  $[\text{amb}_5+\text{Zn(II)}]^-$  (shown in bold in Table 1) to be compared with the TWIMMS  $\Omega_{\text{He}}$  distributions (Fig 4). Figure 4a compares the  $\text{amb}_{5\text{S}}$  complexes, which show the TWIMMS and MD exhibit distributions centered around the average  $\Omega_{\text{He}}$ , but with the MD distributions significantly narrower, exhibiting FWHM = 6  $\text{\AA}^2$  and FWHM = 4  $\text{\AA}^2$  compared to the TWIMMS FWHM = 12  $\text{\AA}^2$  and FWHM = 15  $\text{\AA}^2$  for  $[\text{amb}_{5\text{S}}+\text{Zn(II)+NTA}]^-$  and  $[\text{amb}_{5\text{S}}+\text{Zn(II)}]^-$ , respectively. A comparison of the  $\text{amb}_{5\text{T}}$  complexes also show narrower MD  $\Omega_{\text{He}}$  distributions, FWHM =

5 Å<sup>2</sup> and FWHM = 4 Å<sup>2</sup> compared to the TWIMMS FWHM = 14 Å<sup>2</sup> and FWHM = 13 Å<sup>2</sup> for [amb<sub>5T</sub>+Zn(II)+NTA]<sup>-</sup> and [amb<sub>5T</sub>+Zn(II)]<sup>-</sup>, respectively. The MD Ω<sub>He</sub> distributions are the changes in structural size of the complex isolated in an "implicit" bath by defining a 300 K temperature using the Langevin equations. For the TWIMMS Ω<sub>He</sub> measurement there are additional broadening affects that includes the initial 200 μs injection time of the ions into the IM T-wave cell, followed by deflections of the ions into slightly different trajectories by collisions with the N<sub>2</sub> buffer gas as they are pushed through the IM T-wave cell by the traveling waves. The T-wave heights and velocities in this study kept the time distribution minimal, *e.g.*, for [amb<sub>5S</sub>+Zn(II)+NTA]<sup>-</sup> the final time distribution was FWHM = 800 μs.

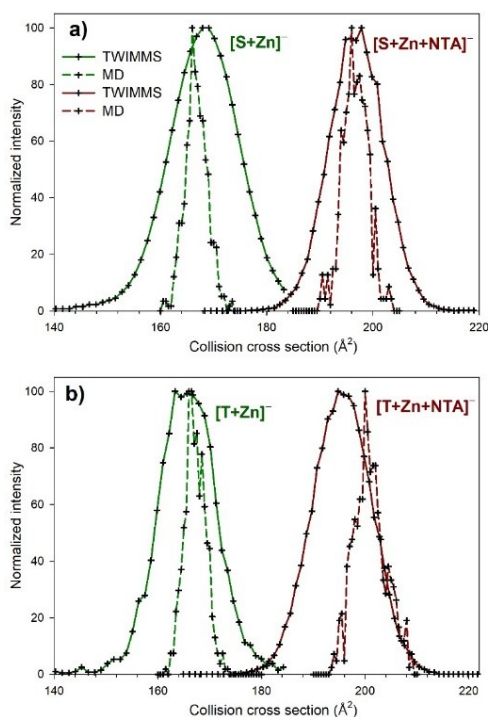


**Figure 4.** The comparison of the TWIMMS collision cross section distributions of the [amb<sub>5</sub>+Zn(II)+NTA]<sup>-</sup> complexes and their products [amb<sub>5</sub>+Zn(II)]<sup>-</sup> with the collision cross section distributions from the molecular dynamics (MD) simulations of the DFTB/3OB\_D4 conformers.

Another contribution to the broader TWIMMS Ω<sub>He</sub> distributions could be the average temperature of the complexes in the IM T-wave cell being on average hotter than the 300 K used in the MD simulations. A previous study<sup>46</sup> of the temperature of peptide ions in the IM T-wave cell of the G2 Synapt instrument indicated that the initial injection resulted in collisions with the nitrogen buffer gas that internally excited the peptide ions to 449 K, before they passed down the IM T-wave cell and the

subsequent lower energy collisions thermalized them to the 300 K temperature of the nitrogen buffer gas before exiting the IM T-wave cell. The broader widths of the TWIMMS  $\Omega_{\text{He}}$  distributions could also indicate the presence of multiple conformers with similar  $\Omega_{\text{He}}$  and the distribution includes a summation of these distributions. In principle a trajectory long enough to sample the phase space available at the given thermodynamics conditions should include the contribution of multiple conformers, however the limitation in simulation time-length due to computational reasons is typically at the origin of an insufficient sampling. To contour this problem, we have run trajectories using as initial geometries different conformers, calculate the respective  $\Omega_{\text{He}}$  and associated distributions and summed them. Figure 5 shows the comparison of the TWIMMS  $\Omega_{\text{He}}$  distribution of the  $[\text{amb}_{55}+\text{Zn}(\text{II})+\text{NTA}]^-$  complex with the L-J  $\Omega_{\text{He}}$  distributions from the MD simulations using as starting geometries the three DFTB/3OB\_D4 conformers S2a, S2b, and S2c (Table 1). If the abundances of the conformers S2a and b are 55% relative to the 100% conformer S2c then a reasonably good reproduction of the TWIMMS  $\Omega_{\text{He}}$  distribution would be obtained with the summation of all three of these L-J  $\Omega_{\text{He}}$  distributions, indicating these three conformers could be present in the experiment. The following TCID analyses will use the DFTB/3OB\_D4 conformers selected in bold from Table 1, and in the Supporting Information a selection of the PM6 conformers from Table 1 will be used to ascertain how these different conformer's vibrational frequencies affect the final TCID threshold analyses.

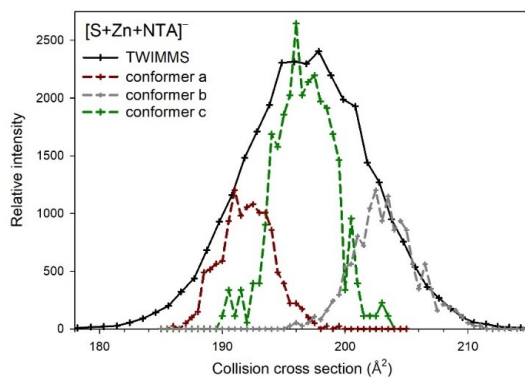


**Figure 5.** The comparison of the TWIMMS collision cross section distribution of the  $[\text{amb}_{55}+\text{Zn}(\text{II})+\text{NTA}]^-$  complex with the collision cross section distributions from the molecular dynamics simulations of the three conformers S2a, S2b, and S2c geometry-optimized by DFTB/3OB\_D4. The relative abundances of conformers S2a = b = 55% and conformer c = 100%.

Figure 6 shows the DFTB/3OB\_D4 conformers selected for the TCID modeling of the dissociation of the  $[\text{amb}_{55}+\text{Zn(II)}+\text{NTA}]^-$  complex into the products  $[\text{amb}_{55}+\text{Zn(II)}]^- + \text{NTA}$  (right) and  $[\text{NTA}+\text{Zn(II)}]^- + \text{amb}_{55}$  (left). The L-J  $\Omega_{\text{He}}$  for  $[\text{amb}_{55}+\text{Zn(II)}+\text{NTA}]^-$  and  $[\text{amb}_{55}+\text{Zn(II)}]^-$  (Table 1, Fig 4a) were in best agreement with the TWIMMS  $\Omega_{\text{He}}$ . The  $\text{amb}_{55}$ , NTA and  $[\text{NTA}+\text{Zn(II)}]^-$  conformers were the lowest energy conformers located, because their  $\Omega_{\text{He}}$  could not be measured by the PA calibration;  $\text{amb}_{55}$  and NTA are neutral species and  $[\text{NTA}+\text{Zn(II)}]^-$  was too small in size.

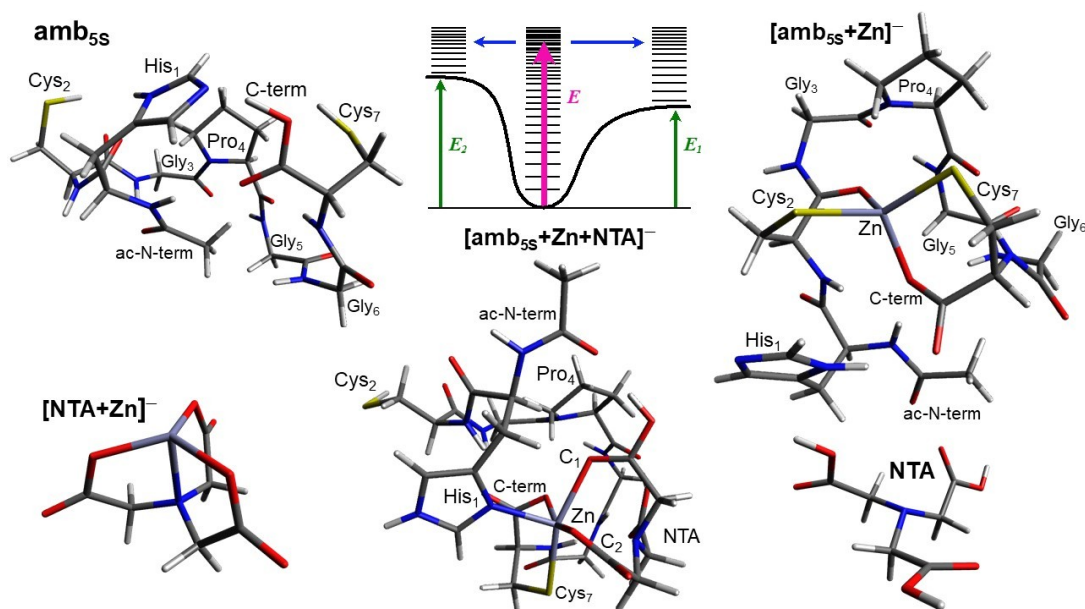


**Figure 6.** The DFTB/3OB\_D4 conformers of the  $[\text{amb}_{55}+\text{Zn(II)}+\text{NTA}]^-$  ternary complex and the products  $[\text{amb}_{55}+\text{Zn(II)}]^- + \text{NTA}$  (right) and  $[\text{NTA}+\text{Zn(II)}]^- + \text{amb}_{55}$  (left). The molecular parameters of these conformers were used in the modelling of the TCID reaction to extract the 0 K threshold energies. The representative potential energy surface illustrates the density of states of the energized  $[\text{amb}_{55}+\text{Zn(II)}+\text{NTA}]^-$  complex and the sum of states of the two product channels. The threshold energies,  $E_1$  and  $E_2$ , indicate the 0 K enthalpy changes for the two reactions.

The DFTB/3OB\_D4 conformer  $[\text{amb}_{55}+\text{Zn(II)}+\text{NTA}]^-$  has the substituent groups of His<sub>1</sub>, Cys<sub>7</sub> and the carboxylate terminus (C-terminus), with a carboxyl (C<sub>1</sub>) and carboxylate (C<sub>2</sub>) from the NTA, occupying five sites of a distorted octahedral Zn(II) coordination geometry. The three negatively charged sites of Cys<sub>7</sub>, C-terminus and the carboxylate (C<sub>2</sub>) with the 2+ charge from Zn(II) gives the overall -1 charge of the ternary complex. For  $[\text{amb}_{55}+\text{Zn(II)}]^-$  the Zn(II) the substituent groups of Cys<sub>2</sub> and Cys<sub>7</sub>, backbone carbonyl group of Cys<sub>2</sub>, and C-terminus coordinated Zn(II) in a distorted tetrahedral geometry. The reaction mechanism for the  $[\text{amb}_{55}+\text{Zn(II)}+\text{NTA}]^-$  conformer to dissociate into the  $[\text{amb}_{55}+\text{Zn(II)}]^- +$

NTA conformers must proceed via a proton transfer from Cys<sub>2</sub> to NTA and the backbone carboxyl and thiolate groups of Cys<sub>2</sub> replacing the His<sub>1</sub> coordinating Zn(II).

Figure 7 shows the DFTB/3OB\_D4 conformers of [amb<sub>5T</sub>+Zn(II)+NTA]<sup>-</sup> and the products [amb<sub>5T</sub>+Zn(II)]<sup>-</sup> + NTA (right) and [NTA+Zn(II)]<sup>-</sup> + amb<sub>5T</sub> (left) selected for the TCID modeling. The [amb<sub>5T</sub>+Zn(II)+NTA]<sup>-</sup> complex exhibits Asp<sub>1</sub> and Cys<sub>7</sub> coordination of Zn(II) and amine and two carboxylates (C<sub>1</sub> and C<sub>2</sub>) from NTA in a distorted bipyramidal geometry. These are the four negatively-charged sites that are balanced by the Zn(II) ion and His<sub>2</sub> imidazolium group to give the overall -1 charge of the complex. The [amb<sub>5T</sub>+Zn(II)]<sup>-</sup> complex exhibits Asp<sub>1</sub>, His<sub>2</sub>, Cys<sub>7</sub>, and C-terminus coordination of Zn(II) via a distorted tetrahedral geometry. The dissociation of [amb<sub>5T</sub>+Zn(II)+NTA]<sup>-</sup> into the [amb<sub>5T</sub>+Zn(II)]<sup>-</sup> conformer requires proton transfers from His<sub>2</sub> and the carboxyl terminus to the two carboxylate sites (C<sub>1</sub> and C<sub>2</sub>) of NTA, which His<sub>2</sub> and the C-terminus will subsequently displace in coordinating Zn(II).

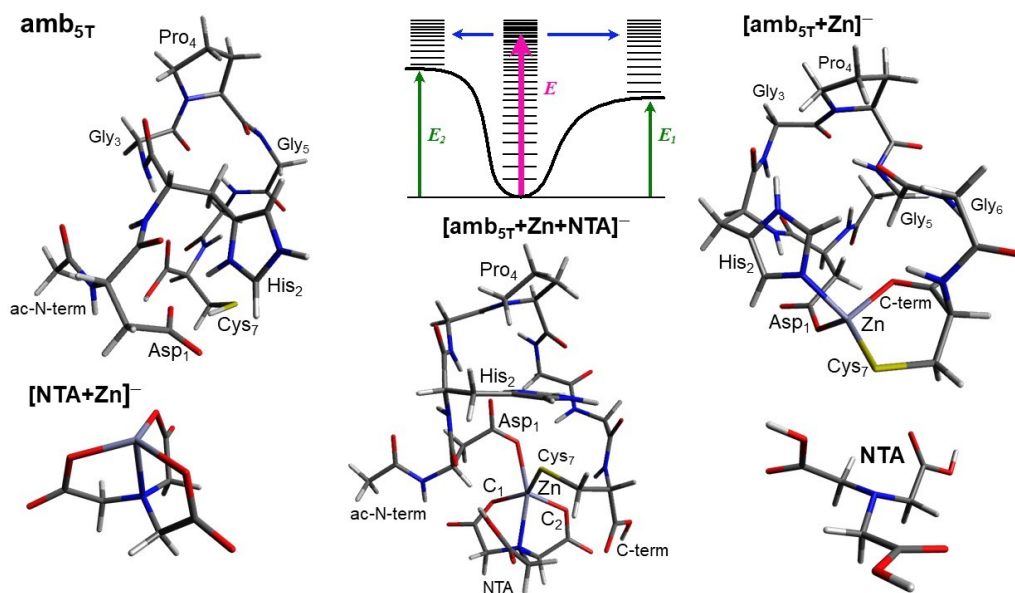


**Figure 7.** The DFTB/3OB\_D4 conformers used in the TCID modeling of the dissociation of the [amb<sub>5T</sub>+Zn(II)+NTA]<sup>-</sup> complex (center) into its products [amb<sub>5T</sub>+Zn(II)]<sup>-</sup> + NTA (right) and [NTA+Zn(II)]<sup>-</sup> + amb<sub>5T</sub> (left). The representative potential energy surface illustrates the energized ternary complex dissociating into the two product channels and indicates the density of states of the ternary complex and the sum of states of the products. The threshold energies,  $E_1$  and  $E_2$ , indicate the 0 K enthalpy changes for the two reactions.

### 3.3 Energy-resolved, threshold collision-induced dissociation of the [amb<sub>5</sub>+Zn(II)+NTA]<sup>-</sup> complex

Figure 8 shows the competitive TCID fits to the  $E_{\text{cm}}$ -dependent  $\sigma_p$  convoluted over the energy distributions available during the reaction. The unconvoluted model (not shown) predicts the threshold behavior at 0 K, which are equal to the 0 K enthalpies of dissociation ( $\Delta H_0$ ) for the reactions 6 and 7.

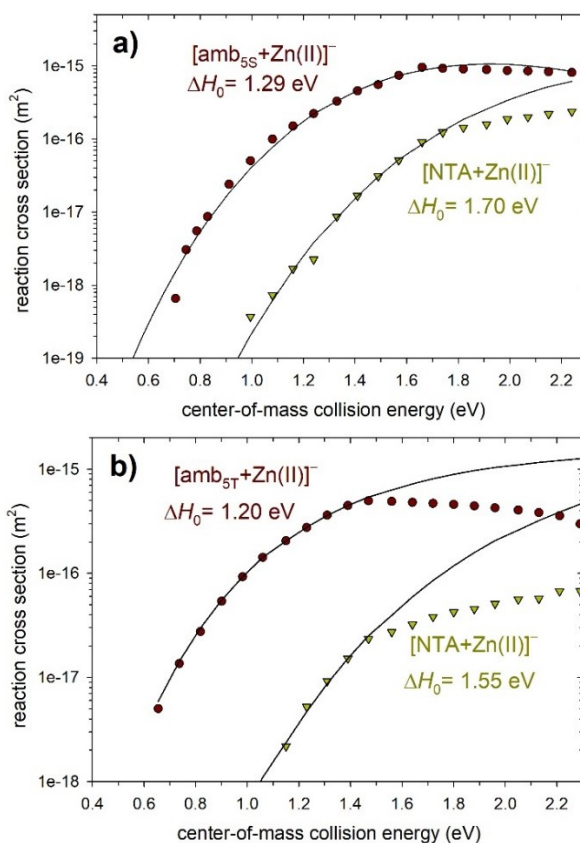
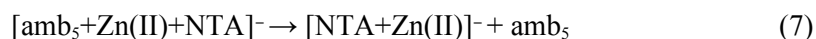


**Figure 8.** The competitive TCID fits of the reaction cross sections of the products  $[\text{amb}_5+\text{Zn(II)}]^-$  and  $[\text{NTA}+\text{Zn(II)}]^-$  (symbols) from the dissociation of **a)**  $[\text{amb}_{5\text{S}}+\text{Zn(II)}+\text{NTA}]^-$  and **b)**  $[\text{amb}_{5\text{T}}+\text{Zn(II)}+\text{NTA}]^-$  over center-of-mass collision energy. The convoluted TCID fits (black lines) include the energy distributions available during the experiment. The 0 K dissociation enthalpies ( $\Delta H_0$ ) are derived from the unconvoluted 0 K model (not shown).

The dissociation of  $[\text{amb}_{5\text{S}}+\text{Zn(II)}+\text{NTA}]^-$  (Fig 8a), shows the  $\sigma_p$  for the ions in the two competing product channels (reactions 6 and 7) with the convoluted TCID fit that reproduces the  $\sigma_p$  over  $E_{\text{cm}} = 0.6\text{-}1.8$  eV, with a deviation at collision energies  $>1.8$  eV for  $[\text{NTA}+\text{Zn(II)}]^-$ . The  $\Delta H_0$  for reaction 6 (1.29 eV) and reaction 7 (1.70 eV) exhibit an 0.41 eV difference between the two competing reactions.

For the dissociation of the ternary complex  $[\text{amb}_{5\text{T}}+\text{Zn(II)}+\text{NTA}]^-$  (Fig 8b) the TCID convoluted model reproduces the  $\sigma_p$  for the  $[\text{amb}_{5\text{T}}+\text{Zn(II)}]^-$  and  $[\text{NTA}+\text{Zn(II)}]^-$  channels over  $E_{\text{cm}} = 0.6 - 1.5$  eV, but departs at higher energies. Some of the deviation may be attributed to the  $[\text{amb}_{5\text{T}}-\text{H}_2\text{O}+\text{Zn(II)}]^-$  channel becoming significant (Fig 3) at these CE and not included in the TCID model. However, from the reproduced threshold regions 0.6 - 1.5 eV for  $[\text{amb}_{5\text{T}}+\text{Zn(II)}]^-$  and  $[\text{NTA}+\text{Zn(II)}]^-$  the unconvoluted 0 K model derived threshold energies equating  $\Delta H_0 = 1.20$  eV for reaction 6 and  $\Delta H_0 = 1.55$  eV for reaction 7, with a 0.35 eV difference between the two reactions.

### 3.4 Evaluation of the TCID thermochemical analysis

The difference in the 0 K changes in enthalpies for the two competing reactions 6 and 7, *i.e.*,  $\delta\Delta_{\text{Zn}}H_0 = \Delta H_0(6) - \Delta H_0(7) = \Delta_{\text{Zn}}H_0(\text{amb}_5) - \Delta_{\text{Zn}}H_0(\text{NTA})$ , is a more consistent measurement than the two absolute  $\Delta H_0$  values, because many of the uncertainties in the TCID measurement cancel out.<sup>12,47</sup> The  $\delta\Delta_{\text{Zn}}H_0$  also provides a relative gas-phase Zn(II) affinity scale for the  $\text{amb}_5$  species studied here and in our previous TCID research based on reactions 6 and 7.<sup>16</sup> Table 2 shows a comparison of the relative  $\delta\Delta_{\text{Zn}}H_0$  using NTA as the baseline and includes the previously studied  $\text{amb}_{5\text{A}}$  and  $\text{amb}_{5\text{H}}$ , which have the common primary structure  $\text{ac-Aa}_1\text{-Cys}_2\text{-Gly}_3\text{-Pro}_4\text{-Tyr}_5\text{-His}_6\text{-Cys}_7$ , where the amino acid  $\text{Aa}_1 = \text{His}_1$  or  $\text{Asp}_1$ , respectively, with  $\text{amb}_{5\text{A}}$  exhibiting a more exothermic Zn(II) affinity than  $\text{amb}_{5\text{H}}$ . The primary structure of  $\text{amb}_{5\text{A}}$  is also closely related to the new  $\text{amb}_{5\text{S}}$  studied here where their primary structures only differ by the  $\text{Tyr}_5\text{-His}_6$  residues being replaced by  $\text{Gly}_5\text{-Gly}_6$ , respectively. This allows the determination of how the substituent groups of  $\text{Tyr}_5\text{-His}_6$  effect the Zn(II) affinity of these two  $\text{amb}_5$  peptides. Table 2 shows the  $\delta\Delta_{\text{Zn}}H_0$  measurement for  $\text{amb}_{5\text{S}}$  using the DFTB conformers (Fig 6) with the two  $\delta\Delta_{\text{Zn}}H_0$  measurements made using the PM6 conformers, with the conformers and TCID fits shown in the Supporting Information (Fig S8, S9 and S11). The range of these three  $\delta\Delta_{\text{Zn}}H_0$  measurements is 0.11 eV, but all three values are twofold or more exothermic than the  $\delta\Delta_{\text{Zn}}H_0$  of  $\text{amb}_{5\text{A}}$ , previously modeled with PM6 conformers.<sup>16</sup> These results clearly indicate that the  $\text{amb}_{5\text{A}}$  substituent groups of  $\text{Tyr}_5\text{-His}_6$  decrease the Zn(II) affinity in respect to the  $\text{amb}_{5\text{S}}$ . The Tyr residue was originally included in the primary structure of the  $\text{amb}$  peptides

because its substituent group could provide a stabilizing  $\pi$  - zinc cation interaction and spectroscopic tag for absorbance and fluorescence studies.<sup>21,29</sup> However, the results here suggests that steric effects from the bulky Tyr side group are detrimental to Zn(II) binding at least for these amb<sub>5</sub> peptides. The loss of Zn(II) affinity from the imidazole of His<sub>6</sub> indicates that the imidazole does not provide a Zn(II) binding site. This is consistent with our previous amb research that showed the Zn(II) binding sites are the substituent groups in the first two positions, *e.g.*, His<sub>1</sub>-Cys<sub>2</sub>, and the combination of the thiolate of Cys in the last position with the carboxylate terminus that provided the four coordination sites for the distorted tetrahedral geometry.<sup>24,27</sup> The  $\delta\Delta_{Zn}H_0$  measurements of amb<sub>5S</sub> are also more exothermic than the  $\delta\Delta_{Zn}H_0$  measurements of amb<sub>5T</sub>, which used the DFTB conformers (Fig 7, 8b) or PM6 conformers (Fig S10, S12), indicating the His<sub>1</sub>-Cys<sub>2</sub> substituent groups of amb<sub>5S</sub> have a higher Zn(II) affinity than the Asp<sub>1</sub>-His<sub>2</sub> of amb<sub>5T</sub>. The amb<sub>5T</sub> also exhibits a higher Zn(II) affinity than the amb<sub>5A</sub> and amb<sub>5H</sub> which both contain the Tyr<sub>5</sub>-His<sub>6</sub> residues whereas, amb<sub>5T</sub> contains the Gly<sub>5</sub>-Gly<sub>6</sub> sequence. **Add discussion of amb5- and His-Cys-C-term salt-bridges and C-term-Tyr hydrogen bond.**

**Table 2.** Comparison of the difference in the competitive TCID 0 K enthalpies ( $\Delta H_0$ ) for reactions 6 and 7 shown in the script. The difference,  $\delta\Delta_{Zn}H_0 = \Delta H_0(6) - \Delta H_0(7) = \Delta_{Zn}H_0(\text{amb}_5) - \Delta_{Zn}H_0(\text{NTA})$ , gives a relative gas-phase Zn(II) affinity scale for the amb<sub>5</sub> species studied here and in our previous research.<sup>16</sup>

Name: primary structure or formula	$\delta\Delta_{Zn}H_0$ (eV)
<b>amb<sub>5S</sub></b> : ac-His-Cys-Gly-Pro-Gly-Gly-Cys	-0.41 (-0.44, -0.52) <sup>1</sup>
<b>amb<sub>5T</sub></b> : ac-Asp-His-Gly-Pro-Gly-Gly-Cys	-0.35 (-0.40) <sup>1</sup>
<b>amb<sub>5A</sub></b> : ac-His-Cys-Gly-Pro-Tyr-His-Cys	-0.22
<b>amb<sub>5H</sub></b> : ac-Asp-Cys-Gly-Pro-Tyr-His-Cys	-0.15
<b>NTA</b> : N(CH <sub>2</sub> COOH) <sub>3</sub>	0

<sup>1</sup> In brackets are the differences in  $\delta\Delta_{Zn}H_0$  measured by TCID using the PM6 molecular parameters shown in the Supporting Information in Figures S8, S9, S10, S11 and S12.

#### 4. Conclusions

This research further extended the competitive TCID methodologies using the traveling-wave ion mobility-mass spectrometry (TWIMMS) platform<sup>17</sup> and whether it provides the relative gas-phase Zn(II) affinities for alternative metal binding (amb) heptapeptides. The competitive TCID analyses was applied

to the dissociation of two  $[\text{amb}_5+\text{Zn}(\text{II})+\text{NTA}]^-$  ternary complexes containing either  $\text{amb}_{5\text{SS}}$  and  $\text{amb}_{5\text{ST}}$  using the CRUNCH reaction dynamics program.<sup>4</sup> The  $\text{amb}_{5\text{SS}}$  and  $\text{amb}_{5\text{ST}}$  had simplified primary structures to those studied previously to test whether the  $\text{Zn}(\text{II})$  affinity were affected by replacing  $\text{Tyr}_5\text{-His}_6$  with  $\text{Gly}_5\text{-Gly}_6$  from the  $\text{amb}_5$  structure.<sup>24,27</sup> The analyses included converting ion intensities into product reaction cross sections which are extrapolated to the single collision limit, and the application of a new theoretical approach for selecting the reactant and product conformers to use in the TCID modeling. The competitive TCID analyses required the vibrational and rotational frequencies for the ternary complex and their dissociation products, including polarizabilities and dipole moments of the neutral products. This new method included theoretical calculations to identify the structures of the ions by comparing theoretical with experimental collision cross sections by (i) identifying conformers from PM6 geometry optimization and frequency calculations; (ii) using an ensemble of structures sampled by molecular dynamics simulations using tight-binding Density Functional Theory.

The TCID analyses included using alternative sets of conformers to test their effect on the dissociation reactions  $\Delta H_0$  and the  $\text{amb}_5$  relative gas-phase  $\text{Zn}(\text{II})$  affinities. The maximum range of  $\text{Zn}(\text{II})$  affinities was 0.11 eV using three sets of alternative sets conformers and was consistent enough to be able to determine differences in the relative  $\text{Zn}(\text{II})$  affinities of the two  $\text{amb}_5$  species studied here and two from our previous competitive TCID analyses. The results revealed that the substituent groups of  $\text{Tyr}_5\text{-His}_6$  decreased the  $\text{Zn}(\text{II})$  affinity. For  $\text{Tyr}_5$  the potential of providing a second-shell stabilizing  $\pi$  - zinc cation interaction seems to be out-weighed by steric effects interfering with the first-shell  $\text{Zn}(\text{II})$  coordination. The loss of  $\text{Zn}(\text{II})$  affinity from imidazole of  $\text{His}_6$  also indicated that this imidazole does not bind in the first shell to the  $\text{Zn}(\text{II})$ , consistent with our previous research<sup>24,27</sup> indicating the  $\text{Zn}(\text{II})$  binding sites are either the His, Cys, or Asp in the first two positions of the primary structure and the combination of the thiolate of  $\text{Cys}_7$  and its carboxylate terminus binding the  $\text{Zn}(\text{II})$  in a distorted tetrahedral coordination geometry.

## Acknowledgements

This work was supported by the National Science Foundation (1764436), NSF REU program (CHE-1659852), NSF instrument support (MRI-0821247), and Welch Foundation (T-0014). We thank Kent M. Ervin (University of Nevada - Reno) and Peter B. Armentrout (University of Utah) for sharing the CRUNCH program. We also thank Michael T. Bowers (University of California - Santa Barbara) for sharing the Sigma program.

## References

1. Armentrout, P.B., Ervin, K.M., and Rodgers, M.T. (2008) Statistical Rate Theory and Kinetic Energy-Resolved Ion Chemistry: Theory and Applications. *J. Phys. Chem. A* **112**, 10071-10085.
2. Rodgers, M.T., and Armentrout, P.B. (1998) Statistical modeling of competitive threshold collision-induced dissociation. *J. Chem. Phys.* **109**, 1787-1800.
3. Rodgers, M.T., Ervin, K.M., and Armentrout, P.B. (1997) Statistical modeling of collision-induced dissociation thresholds. *J. Chem. Phys.* **106**, 4499-4508.
4. Armentrout, P.B., and Ervin, K.M. (2016) CRUNCH, Fortran program, version 5.2002.
5. Roy, H.A., and Rodgers, M.T. (2021) 1-Alkyl-3-methylimidazolium cation binding preferences in hexafluorophosphate ionic liquid clusters determined using competitive TCID measurements and theoretical calculations. *Phys. Chem. Chem. Phys.* **23**, 18145-18162.
6. Roy, H.A., and Rodgers, M.T. (2020) Absolute Trends and Accurate and Precise Gas-Phase Binding Energies of 1-Alkyl-3-Methylimidazolium Tetrafluoroborate Ionic Liquid Clusters from Combined Independent and Competitive TCID Measurements. *J. Phys. Chem. A* **124**, 10199-10215.
7. Mookherjee, A., and Armentrout, P.B. (2019) Thermodynamics and Reaction Mechanisms for Decomposition of a Simple Protonated Tripeptide, H<sup>+</sup>GAG: a Guided Ion Beam and Computational Study. *J. Am. Soc. Mass Spectrom.* **30**, 1013-1027.
8. Mookherjee, A., Van Stipdonk, M.J., and Armentrout, P.B. (2017) Thermodynamics and Reaction Mechanisms of Decomposition of the Simplest Protonated Tripeptide, Triglycine: A Guided Ion Beam and Computational Study. *J. Am. Soc. Mass Spectrom.* **28**, 739-757.
9. Amicangelo, J.C.; Armentrout, P.B. (2001) Relative and absolute bond dissociation energies of sodium cation complexes determined using competitive collision-induced dissociation experiments. *Int. J. Mass Spectrom.*, **212**, 301-325.
10. Chen, Y., Rodgers, M.T. (2012) Re-Evaluation of the Proton Affinity of 18-Crown-6 Using Competitive Threshold Collision-Induced Dissociation Techniques. *Anal. Chem.*, **84**, 7570-7577.
11. Jia, B., Angel, L.A., and Ervin, K.M. (2008) Threshold Collision-Induced Dissociation of Hydrogen-Bonded Dimers of Carboxylic Acids. *J. Phys. Chem. A* **112**, 1773-1782.
12. Angel, L.A., and Ervin, K.M. (2006) Gas-phase acidities and O-H bond dissociation enthalpies of phenol, 3-methylphenol, 2,4,6-trimethylphenol, and ethanoic acid. *J. Phys. Chem. A* **110**, 10392-10403.
13. Amicangelo, J.C.; Armentrout, P.B. (2001) Re-Evaluation of the Proton Affinity of 18-Crown-6 Using Competitive Threshold Collision-Induced Dissociation Techniques. *Int. J. Mass Spectrom.*, **212**, 301-325.
14. DeTuri, V.F., and Ervin, K.M. (1999) Competitive Threshold Collision-Induced Dissociation: Gas-Phase Acidities and Bond Dissociation Energies for a Series of Alcohols. *J. Phys. Chem. A* **103**, 6911-6920.

15. Flores, A.A., Arredondo, A.V., Corrales, A.J., Duvak, C.L., Mitchell, C.L., Falokun, O., Aguilar, C.L., Kim, A., Daniel, B.C., Karabulut, H.D., Spezia, R., and Angel, L.A. (2022) Thermochemical and conformational studies of Ni(II) and Zn(II) ternary complexes of alternative metal binding peptides with nitrilotriacetic acid. *Int. J. Mass Spectrom.* **473**, 116792.
16. Corrales, A.J., Arredondo, A.V., Flores, A.A., Duvak, C.L., Mitchell, C.L., Spezia, R., and Angel, L.A. (2022) Thermochemical Studies of Ni(II) and Zn(II) Ternary Complexes using Ion Mobility-Mass Spectrometry. *J. Visualized Exp.*, e63722.
17. Pringle, S.D., Giles, K., Wildgoose, J.L., Williams, J.P., Slade, S.E., Thalassinou, K., Bateman, R.H., Bowers, M.T., and Scrivens, J.H. (2007) An investigation of the mobility separation of some peptide and protein ions using a new hybrid quadrupole/travelling wave IMS/oa-ToF instrument. *Int. J. Mass Spectrom.* **261**, 1-12.
18. Tao, L., Dahl, D.B., Pérez, L.M., and Russell, D.H. (2009) The contributions of molecular framework to IMS collision cross-sections of gas-phase peptide ions. *J. Am. Soc. Mass Spectrom.* **20**, 1593-1602.
19. Lim, D., Park, Y., Chang, R., Ahmed, A., and Kim, S. (2019) Application of molecular dynamics simulation to improve the theoretical prediction for collisional cross section of aromatic compounds with long alkyl chains in crude oils. *Rapid Commun. Mass Spectrom.* **33**, 650-656.
20. Sesham, R., Choi, D., Balaji, A., Cheruku, S., Ravichetti, C., Alshahrani, A.A., Nasani, M., and Angel, L.A. (2013) The pH dependent Cu(II) and Zn(II) binding behavior of an analog methanobactin peptide. *Eur. J. Mass Spectrom.* **19**, 463-473.
21. Choi, D., Alshahrani, A.A., Vytla, Y., Deconada, M., Serna, V.J., Saenz, R.F., and Angel, L.A. (2015) Redox activity and multiple copper(I) coordination of 2His-2Cys oligopeptide. *J. Mass Spectrom.* **50**, 316-325.
22. Wagoner, S.M., Deconada, M., Cumpian, K.L., Ortiz, R., Chinthala, S., and Angel, L.A. (2016) The multiple conformational charge states of zinc(II) coordination by 2His-2Cys oligopeptide investigated by ion mobility - mass spectrometry, density functional theory and theoretical collision cross sections. *J. Mass Spectrom.* **51**, 1120-1129.
23. Vytla, Y., and Angel, L.A. (2016) Applying Ion Mobility-Mass Spectrometry Techniques for Explicitly Identifying the Products of Cu(II) Reactions of 2His-2Cys Motif Peptides. *Anal. Chem.* **88**, 10925-10932.
24. Lin, Y.-F., Yousef, E.N., Torres, E., Truong, L., Zahnow, J.M., Donald, C.B., Qin, Y., and Angel, L.A. (2019) Weak acid-base interactions of histidine and cysteine affect the charge states, tertiary structure, and Zn(II)-binding of heptapeptides. *J. Am. Soc. Mass Spectrom.* **30**, 2068-2081.
25. Yousef, E.N., Sesham, R., McCabe, J.W., Vangala, R., and Angel, L.A. (2019) Ion mobility-mass spectrometry techniques for determining the structure and mechanisms of metal ion recognition and redox activity of metal binding oligopeptides. *J. Visualized Exp.*, e60102.
26. Yousef, E.N., and Angel, L.A. (2020) Comparison of the pH-dependent formation of His and Cys heptapeptide complexes of nickel(II), copper(II), and zinc(II) as determined by ion mobility-mass spectrometry. *J. Mass Spectrom.* **55**, e4489.
27. Ilesanmi, A.B., Moore, T.C., and Angel, L.A. (2020) pH dependent chelation study of Zn(II) and Ni(II) by a series of hexapeptides using electrospray ionization - Ion mobility - Mass spectrometry. *Int. J. Mass Spectrom.* **455**, 116369.
28. Flores, A.A., Falokun, O.S., Ilesanmi, A.B., Arredondo, A.V., Truong, L., Fuentes, N., Spezia, R., and Angel, L.A. (2021) Formation of Co(II), Ni(II), Zn(II) complexes of alternative metal binding heptapeptides and nitrilotriacetic acid: Discovering new potential affinity tags. *Int. J. Mass Spectrom.* **463**, 116554.

29. Vangala, R., and Angel, L.A. (2021) ESI-IM-MS reveals the metal binding of three analog methanobactin peptides with different numbers of free Cys at physiological pH. *Int. J. Mass Spectrom.* **468**, 116640.
30. Wyttenbach, T., von Helden, G., Batka, J.J., Jr., Carlat, D., and Bowers, M.T. (1997) Effect of the long-range potential on ion mobility measurements. *J. Am. Soc. Mass Spectrom.* **8**, 275-282.
31. Stewart, J.J.P. (2007) Optimization of parameters for semiempirical methods V: Modification of NDDO approximations and application to 70 elements. *Journal of Molecular Modeling* **13**, 1173-1213.
32. Frisch, M.J., Trucks, G.W., Schlegel, H.B., Scuseria, G.E., Robb, M.A., Cheeseman, J.R., Scalmani, G., Barone, V., Mennucci, B., Petersson, G.A., Nakatsuji, H., Caricato, M., Li, X., Hratchian, H.P., Izmaylov, A.F., Bloino, J., Zheng, G., Sonnenberg, J.L., Hada, M., Ehara, M., Toyota, K., Fukuda, R., Hasegawa, J., Ishida, M., Nakajima, T., Honda, Y., Kitao, O., Nakai, H., Vreven, T., Montgomery, J., J. A., Peralta, J.E., Ogliaro, F., Bearpark, M., Heyd, J.J., Brothers, E., Kudin, K.N., Staroverov, V.N., Kobayashi, R., Normand, J., Raghavachari, K., Rendell, A., Burant, J.C., Iyengar, S.S., Tomasi, J., Cossi, M., Rega, N., Millam, J.M., Klene, M., Knox, J.E., Cross, J.B., Bakken, V., Adamo, C., Jaramillo, J., Gomperts, R., Stratmann, R.E., Yazyev, O., Austin, A.J., Cammi, R., Pomelli, C., Ochterski, J.W., Martin, R.L., Morokuma, K., Zakrzewski, V.G., Voth, G.A., Salvador, P., Dannenberg, J.J., Dapprich, S., Daniels, A.D., Farkas, Ö., Foresman, J.B., Ortiz, J.V., Cioslowski, J., and Fox, D.J. (2012) Gaussian 09, Revision C.01. Wallingford CT: Gaussian, Inc.
33. Gaus, M., Goez, A., and Elstner, M. (2013) Parametrization and Benchmark of DFTB3 for Organic Molecules. *J. Chem. Theory Comput.*, **9**, 338-354.
34. Gaus, M., Lu, X., Elstner, M., and Cui, Q. (2014) Parameterization of DFTB3/3OB for Sulfur and Phosphorus for Chemical and Biological Applications. *J. Chem. Theory Comput.*, **10**, 1518-1537.
35. Lu, X., Gaus, M., Elstner, M., and Cui, Q. (2015) Parametrization of DFTB3/3OB for Magnesium and Zinc for Chemical and Biological Applications. *J. Phys. Chem. B*, **119**, 1062-1082.
36. Caldeweyher, E., Bannwarth, C., and Grimme, S. (2017) Extension of the D3 dispersion coefficient model. *J. Chem. Phys.* **147**, 034112.
37. Caldeweyher, E., Ehlert, S., Hansen, A., Neugebauer, H., Spicher, S., Bannwarth, C., and Grimme, S. (2019) A generally applicable atomic-charge dependent London dispersion correction. *J. Chem. Phys.* **150**, 154122.
38. Angiolari, F., Huppert, S., and Spezia, R. (2022) Quantum versus Classical Unimolecular Fragmentation Rate Constants and Activation Energies at Finite Temperature from Direct Dynamics Simulations. *Phys. Chem. Chem. Phys.* **24**, 29357-29370.
39. Ceriotti, M., Parrinello, M., Markland, T. E., and Manolopoulos, D. E. (2010) Efficient stochastic thermostating of path integral molecular dynamics. *J. Chem. Phys.*, **133**, 124104.
40. Craig, I.R., and Manolopoulos, D.E. (2004) Quantum statistics and classical mechanics: Real time correlation functions from ring polymer molecular dynamics. *J. Chem. Phys.*, **121**, 3368.
41. Hourahine, B., Aradi, B., Blum, V., Bonafé, F., Buccheri, A., Camacho, C., Cevallos, C., Deshayé, M.Y., Dumitrică, T., Dominguez, A., Ehlert, S., Elstner, M., van der Heide, T., Hermann, J., Irle, S., Kranz, J. J., Köhler, C., Kowalczyk, T., Kubař, T., Lee, I.S., Lutsker, V., Maurer, R.J., Min, S.K., Mitchell, I., Negre, C., Niehaus, T.A., Niklasson, A.M.N., Page, A.J., Pecchia, A., Penazzi, G., Persson, M.P., Řezáč, J., Sánchez, C.G., Sternberg, M., Stöhr, M., Stuckenberg, F., Tkatchenko, A., Yu, V. W.-z., and Frauenheim, T. (2020) DFTB+, a software package for efficient approximate density functional theory based atomistic simulations. *J. Chem. Phys.* **152**, 124101.

42. DeTuri, V.F.; Hintz, P.A.; Ervin, K.M. (1997) Translational Activation of the  $S_N2$  Nucleophilic Displacement Reactions  $Cl^- + CH_3Cl (CD_3Cl) \rightarrow ClCH_3 (ClCD_3) + Cl^-$ : A Guided Ion Beam Study. *J. Phy. Chem. A*, **101**, 5969-5986.
43. Dalleska, N.F., Honma, K., Sunderlin, L.S., and Armentrout, P.B. (1994) Solvation of Transition Metal Ions by Water. Sequential Binding Energies of  $M^+(H_2O)_x$  ( $x = 1-4$ ) for  $M = Ti$  to  $Cu$  Determined by Collision-Induced Dissociation. *J. Am. Chem. Soc.* **116**, 3519-3528.
44. Ervin, K.M., and Armentrout, P.B. (1985) Translational energy dependence of  $Ar^+ + XY \rightarrow ArX^+ + Y$  ( $XY = H_2, D_2, HD$ ) from thermal to 30 eV c.m. *J. Chem. Phys.* **83**, 166-189.
45. Iceman, C., and Armentrout, P.B. (2003) Collision-induced dissociation and theoretical studies of  $K^+$  complexes with ammonia: a test of theory for potassium ions. *Int. J. Mass Spectrom.* **222**, 329-349.
46. Merenbloom, S. I., Flick, T. G., Williams, E. R. (2012) How Hot are Your Ions in TWAVE Ion Mobility Spectrometry? *J. Am. Soc. Mass Spectrom.* **23**, 553-562.
47. Ervin, K.M. (2001) Experimental Techniques in Gas-Phase Ion Thermochemistry. *Chem. Rev.* **101**, 391-444.